Pure Appl. Geophys.

DOI 10.1007/s00024-014-0823-x

Pure and Applied Geophysics

Stress Patterns in Northern Iraq and Surrounding Regions from Formal Stress Inversion of Earthquake Focal Mechanism Solutions

Wathiq Abdulnaby,[1] Hanan Mahdi,[2] Haydar Al-Shukri,[3] and Nazar M. S. Numan[4]

Abstract—The collision zone between the Arabian and Eurasian plates is one of the most seismically active regions. Northern Iraq represents the northeastern part of the Arabian plate that has a suture zone with the Turkish and Iranian plates called the Bitlis–Zagros suture zone. The orientations of the principal stress axes can be estimated by the formal stress inversion of focal mechanism solutions. The waveform moment tensor inversion method was used to derive a focal mechanism solution of 65 earthquakes with magnitudes range from 3.5 to 5.66 in the study area. From focal mechanism solutions, the direction of slip and the orientations of the moment stress axes (*P*, *N*, and *T*) on the causative fault surface during an earthquake were determined. The dataset of the moment stress axes have been used to infer the regional principal stress axes (σ_1, σ_2, and σ_3) by the formal stress inversion method. Two inversion methods, which are the new right dihedron and the rotational optimization methods, were used. The results show that six stress regime categories exist in the study area. However, the most common tectonic regimes are the strike-slip faulting (43.94 %), unspecified oblique faulting (27.27 %), and thrust faulting (13.64 %) regimes. In most cases, the strike-slip movement on the fault surfaces consists of left-lateral (sinistral) movement. The normal faulting is located in one small area and is due to a local tensional stress regime that develops in areas of strike-slip displacements as pull-apart basins. The directions of the horizontal stress axes show that the compressional stress regime at the Bitlis–Zagros suture zone has two directions. One is perpendicular to the suture zone near the Iraq–Iran border and the second is parallel in places as well as perpendicular in others to the suture zone near the Iraq–Turkey border. In addition, the principal stress axes in the Sinjar area near the Iraq–Syria border have a E–W direction. These results are compatible with the tectonic setting of the Arabian–Eurasian continental collision zone and the anticlockwise rotation of the Arabian plate that is evidently responsible for the strike-slip displacements on fault surfaces.

Key words: Focal mechanism solutions, moment tensor inversion, formal stress inversion, moment stress axes, principal stress axes, stress regimes, Arabian plate, Northern Iraq.

1. Introduction

The purpose of this study is to deduce the present-day stress pattern of the Arabian-Eurasian collision zone in northern Iraq and surrounding regions from the formal stress inversion of the earthquake focal mechanism solutions. In addition, this study intends to compare the present-day stress pattern with the paleostress that was reported in previous studies using structural data from the field or/and remote sensing data (e.g., Numan 1984; Al-Jumaily 2004). To achieve this goal, focal mechanism solutions were done for 65 earthquakes with magnitudes of $\geq$3.5 that occurred from 2004 to 2013 in northern Iraq and surrounding regions by using the moment tensor inversion method of Herrmann and Ammon (2004). Focal mechanism solutions of 40 earthquakes were determined in this study and 25 were taken from Abdulnaby *et al*. (2013). The individual moment stress axes, horizontal stress axes, and stress regimes were deduced from the focal mechanisms. Subsequently, the study area was subdivided into eight regional rectangular sub-areas to study regional changes in stress orientation since the stress regime and stress orientation over the entire northern Iraq and adjacent regions are not consistent. The eight sub-areas were demarcated according to the consistency of individual moment stress directions in each one of them.

Stress inversion analysis was applied to each sub-area in order to determine the regional principal stress axes, regional horizontal stress axes, and regional

[1] Geology Department, College of Science, University of Basra, Basra, Iraq. E-mail: wathiq1972@yahoo.com
[2] Graduate Institute of Technology (GIT), University of Arkansas at Little Rock, 2801 South University Ave., Little Rock, AR 72204, USA. E-mail: hhmahdi@ualr.edu
[3] Department of Applied Science, University of Arkansas at Little Rock, 2801 South University Ave., Little Rock, AR 72204, USA. E-mail: hjalshukri@ualr.edu
[4] Department of Applied Geosciences, University of Duhok, Kurdistan Region, Duhok, Iraq. E-mail: nazarnuman@yahoo.com

Published online: 28 March 2014

stress regime for each sub-area. The orientation (azimuth) of the principal horizontal stress axes (S_H and S_h) were calculated from the principal stress axes within each of the sub-areas. After that, the orientations of S_H and S_h were plotted on the map to produce a recent tectonic stress field map of northern Iraq and adjacent regions. We used two different stress inversion methods; these are the Improved Right Dihedron and the Rotational Optimization methods of DELVAUX and SPERNER (2003).

2. *Tectonic Setting*

The northern part of the Arabian plate is surrounded by active tectonic boundaries; these are the seafloor spreading in the Red Sea, the strike-slip faulting which occurs along the Dead Sea Transform Fault, and the collision of the Arabian plate with the Eurasian plate along the Bitlis–Zagros Fold and Thrust Belt (Fig. 1). Northern Iraq is part of the Arabian–Eurasian continental collision zone. REILINGER *et al.* (2006) studied the plate motion models of the Middle East as derived from the global positioning system (GPS). Their measurements were relative to the Eurasian plate. They reported that the northern part of the Arabian plate is moving towards the NNE direction at a rate of about 15 mm/year, the African plate is moving in a northward direction at a rate of about 5 mm/year, the Turkish plate is moving towards the west at a rate of about 21 mm/year, and the Iranian plate is moving towards the NNW at a rate of about 16 mm/year.

The Dead Sea Transform Fault represents the tectonic boundary between the Arabian and African plates. It is a major left-lateral (sinistral) strike-slip fault that accommodates the differential motion between these two plates, with a displacement of about 5–10 mm/year. The Dead Sea Transform Fault is connecting a region of extension in the Red Sea to the Bitlis suture zone to the north. The Turkish plate is moving laterally to the west along two major

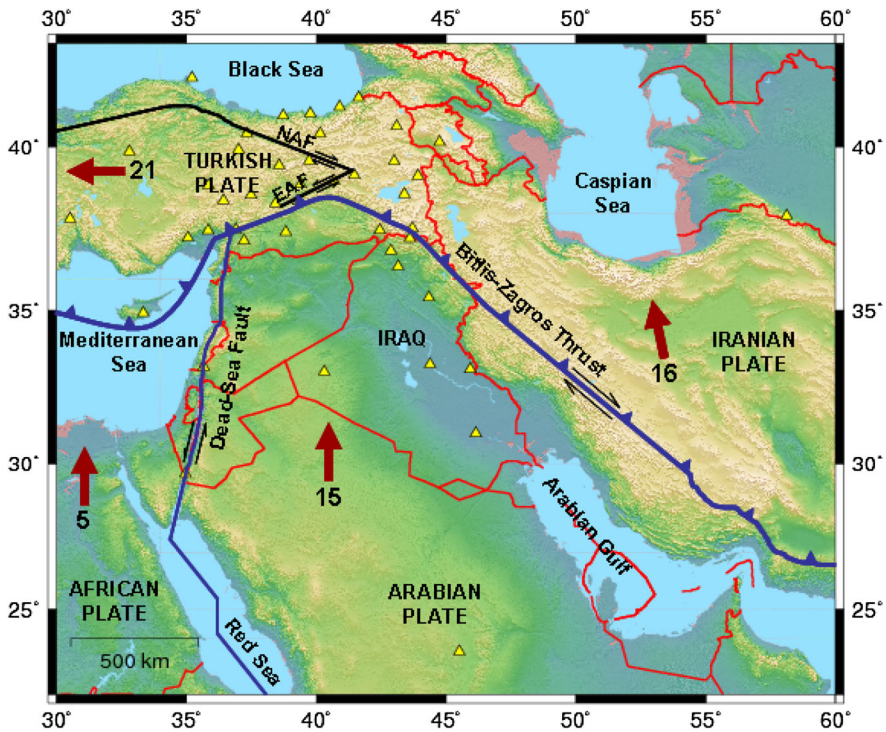

Figure 1
Tectonic map of the Arabian and Eurasian plates. *Yellow triangles* are the broadband seismic stations used in this study. *Brown arrows* and corresponding numbers show the global positioning system (GPS) derived plate velocities (mm/year) relative to Eurasia (modified from ABDULNABY *et al.* 2013; REILINGER 2006)

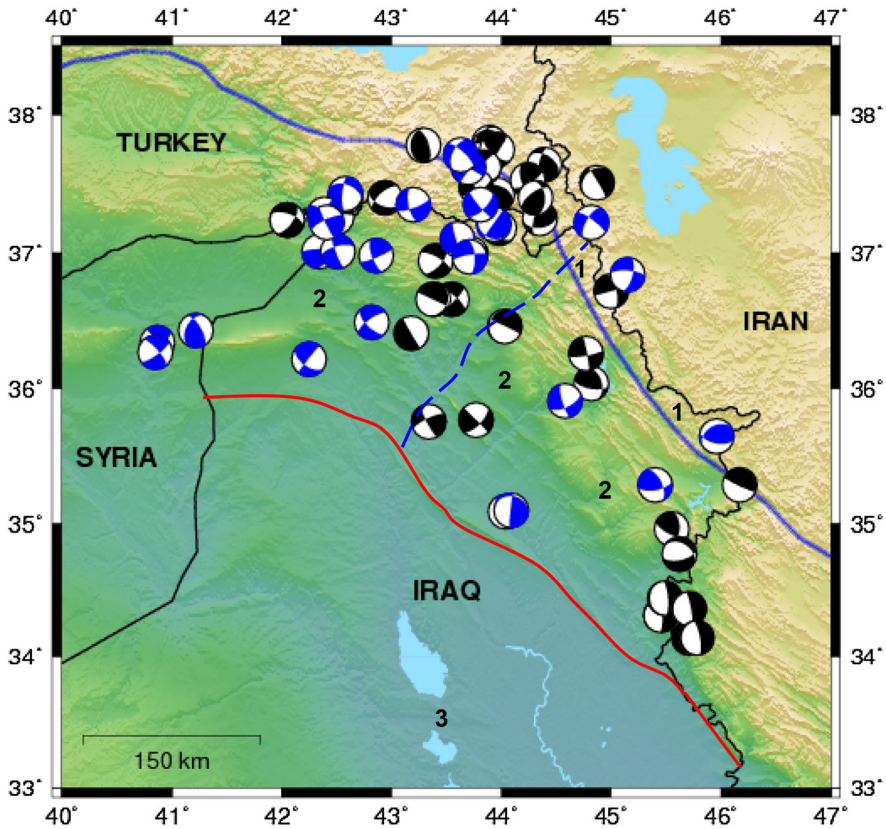

Figure 2
Focal mechanism solutions for 65 earthquakes in northern Iraq shown in a lower hemisphere equal-area projection based on Table 1. *Black beach-balls* are from this study, while *blue beach balls* from Abdulnaby *et al.* (2013). *Solid blue curvy line* is the Bitlis–Zagros suture line. *Solid red curvy lines* represent the tectonic boundary between different tectonic sub-regions. *1* Thrust zone, *2* Foreland fold belt, and *3* Arabian platform. *Broken blue curvy line* represents the Greater Zab Fault

conjugate strike-slip faults; these are the East Anatolian Fault (EAF) and the North Anatolian Fault (NAF).

Our study area is located within the Thrust Zone and the Foreland Folds Belt of the Arabian Plate (Numan 1997, 2000). Fold axes in the Foreland Fold Belt have two distinct trends; these are the E–W trend and NW–SE trend. These trends are separated by the Greater Zab fault. According to Numan (1984), the E–W and NW–SE trends are located within the Mosul and Kirkuk blocks, respectively (Fig. 2). The historical seismicity shows that the seismic activity in the Mosul block is denser than in the Kirkuk block.

3. Datasets

Seismic data of 40 earthquakes with magnitudes of $\geq$3.5 were collected from 54 broadband stations. The epicentral distances between the stations and seismic events ranged from 10 km to 2,000 km. Figure 1 shows the locations of the seismic stations (yellow triangles) that were used for data collections. We used seismic waveform data retrieved from the Kandilli Observatory and Earthquake Research Institute (KOERI), the Incorporated Research Institutions for Seismology (IRIS), the Observatories and Research Facilities for European Seismology (ORFUES), and the Iraqi Seismological Network (ISN). Also, data from Duhok station, which is operated by the Earthquake Center of the University of Arkansas at Little Rock (UALR), was used. The source parameters of the seismic events were selected from the seismic catalog of the European-Mediterranean Seismological Centre (EMSC) and listed in Table 1. We chose this catalog because the source parameters were calculated using local and regional seismic

stations including stations inside Iraq, which will minimize the associated error in location measurements of earthquake epicenters. For more details about the parameters of the seismic stations, see Abdulnaby *et al*. (2013, Table 2).

4. Methods

In this study, the focal mechanism solutions were estimated by using the moment tensor inversion method; and then the orientations of the principal stress axes and the horizontal stress axes were derived from a number of focal mechanisms by using formal stress inversion methods.

4.1. Moment Tensor Inversion Method

The regional moment tensor inversion method was implemented to estimate the focal depths, moment magnitudes, focal mechanism solutions, and directions of moment stress axes of events with magnitudes of $\geq$3.5. The full waveform inversion, which is based on a grid search technique, was used. A package of programs named computer programs in seismology (CPS), version 3.30, developed by Herrmann and Ammon (2002) was used to conduct the moment tensor inversion. In general, the requirements of performing the moment tensor inversion are: waveform data, instrument response, station locations, earthquake location, velocity model, and Green's functions. A flat velocity model was modified from Alsinawi and Al-Heety (1994), Mooney *et al*. (1998), and Abdulnaby *et al*. (2012) to compute Green's functions for northern Iraq and surrounding regions. A good azimuthal coverage around the source is very desirable and critical to such focal mechanism solution studies. However, the majority of seismic data for our study comes from within Iraq or north of Iraq from Turkey with some other few exceptions. Seismic data from Iran and Syria were unavailable to be retrieved. This azimuthal limitation will not affect or bias the results since the complete waveform modeling method is used. This method matches main features in the observed seismograms with the predicted. In this case, more constrain on the depth, strike, dip, rake, and the seismic moment of the earthquake will be taken (Herrmanm and Ammon 1997).

For more details about this method, calculation of the Green's functions and estimating the focal mechanism solutions see Abdulnaby *et al*. (2013), since we used the same technique and procedure. The source parameters were determined by a grid search such that the solution is known within 10° in strike, dip and rake. The grid search does not provide an uncertainty. The final solution depends non-linearly on the azimuthal distribution of observations, the frequency band used, and the velocity model used. To avoid problems of mismatching of peaks and troughs in the waveform inversion, we found a frequency band such that the waveforms were simple, and there was good signal to noise ratio over a wide range of frequencies. This will also minimize the effect of the azimuthal gap on the results. To test the sensitivity of the final mechanism on the data set, we used a leave one out scenario in which we reran the inversion dropping the observations at one station. We found no difference in the results. Also for the sake of accuracy, we did not use precomputed Green functions for the focal mechanism solutions but rather we derived our own regional velocity model, using local and regional data, to be used in the calculation of Greens functions.

4.2. Formal Stress Inversion Methods

The formal stress inversion of moment stress axes (P, N, and T) gives the four parameters of the reduced stress tensor; these are the three principal stress axes (σ_1, σ_2, and σ_3) and the stress ratio $R = (\sigma_2 - \sigma_3)/(\sigma_1 - \sigma_3)$. In this study, two methods of stress inversion are presented; these are the improved right dihedron and the rotational optimization methods.

4.2.1 Improved Right Dihedron Method

Originally, the Right Dihedron method was a graphical method that was developed by Angelier and Mechler (1977) to determine the range of possible orientations of σ_1 and σ_3 stress axes in fault analysis. This method has two limitations. First, it does not determine the stress ratio. Second, it does not define σ_1 and σ_3 when the extreme values on the counting

net do not reach 0 and 100 %. Delvaux and Sperner (2003) developed this method by removing these two limitations and enabled the Improved Right Dihedron method to determine the stress ratio and define σ_1 and σ_3 even under extreme cases (see Delvaux and Sperner 2003 for details). However, the results of this method are used as a starting point for the Rotational Optimization Method.

4.2.2 *Rotational Optimization Method*

This method is a new iterative inversion procedure presented by Delvaux and Sperner (2003). It aims to minimize a misfit function (grid search) based on the testing of a great number of different stress tensors. In this method, both nodal planes for each focal mechanism are inverted to a stress tensor; and the plane that has the smaller value of the misfit from the two nodal planes will be considered as the actual fault plane. This means that we do not need to specify the fault-plane from the auxiliary plane in the inversion routine. After this separation, only the selected fault planes will be inverted to calculate the principal stress axes and the stress ratio. The results will be plotted on an equal-area projection to allow us to evaluate the overall quality of the result.

The Improved Right Dihedron and the Rotational Optimization methods are implemented in a free source program named TENSOR that was developed originally in a DOS operating system by Delvaux (1993). Then it was developed in Windows by Delvaux and Sperner (2003). In this study, the Windows Win-Tensor version 4.0.4 was used to invert the moment stress axes to principal stress axes and stress ratio.

Formal stress inversion of the focal mechanisms data rely on two major assumptions: (a) the stress field is uniform and constant in space and time, and (b) earthquake slip occurs in the direction of maximum shear stress. The angle between the calculated shear stress and the slip vector is the fit angle α. Thus, the corresponding misfit function to be minimized for each individual earthquake is the misfit angle α (Delvaux and Barth 2010)

We process the data interactively, first using the "Improved Right Dihedron Method", for determination of the range of possible orientations σ_1 and σ_3, which is independent from the choice of the nodal planes. This method allows a first estimation of the orientations of the principal stress axes and of the stress ratio R, and a first filtering of compatible fault-slip data (Delvaux and Barth 2010). The selected fault-slip data and the preliminary tensor can be used as a starting point in the iterative grid-search inversion procedures of the Rotational Optimization method which initiates the search procedure using the stress tensor estimated with the Right Dihedron method. It allows restriction of the search area during the inversion, so that the whole grid does not have to be searched (Delvaux and Sperner 2003). It minimizes the misfit angle α using the stress tensor that is being tested, but also favors higher shear stress magnitudes and lower normal stress magnitudes on the plane in order to promote slip (Delvaux and Barth 2010)

5. *Results*

5.1. *Focal Mechanism Solutions*

The output of each focal mechanism solution includes the strike orientation, dip angle, and rake angle for the two plane solutions, which are the fault plane and auxiliary plane. Table 1 lists the moment tensor solutions. Events marked with an asterisk represent focal mechanism solutions that have been derived earlier in Abdulnaby *et al.* (2013). Figure 2 shows the focal mechanism solutions of the 65 events in northern Iraq and surrounding regions.

5.2. *Moment Stress Axes*

In this study, the moment stress axes, which are P, T, and N, were calculated form the focal mechanism solutions and used to study the stress regime in northern Iraq and surrounding regions. Table 1 shows the moment stress axes described by their azimuth (dip direction) and plunge (dip angle). The pressure (P) axis represents the axis of maximum shortening and it is located in the middle of the dilatational quadrant. The tension (T) axis represents the axis of maximum extension, and it is located in the middle of the compressional quadrant. The intermediate

Table 1

Source parameters from the EMSC catalog and moment tensor solutions of the 65 earthquakes from moment tensor inversion

Date	O. time (UTC)	Lat. *N*	Log. *E*	RD (km)	M	CD (km)	M_W	Mo dyne-(cm)	Plane 1			Plane 2			Moment stress axes						S_H	S_h	Stress regime
									S	*D*	*R*	*S*	*D*	*R*	*P*		*N*		*T*				
															PL	AZ	PL	AZ	PL	AZ			
2004/01/10[b]	13:44:58.0	37.78	43.29	05	3.5 MN	21 ± 5	3.60	3.16e+21	340	65	080	183	27	110	19	077	09	344	68	230	081	171	TF
2005/01/25[a]	16:44:09.9	37.54	43.78	10	5.4 mb	16 ± 4	5.66	3.89e+24	120	90	−175	030	85	000	04	345	85	120	04	255	165	075	SS
2005/01/25	17:11:09.1	37.70	43.80	32	4.2 MD	24 ± 8	4.25	2.99e+22	189	66	129	305	45	035	12	251	35	350	52	145	067	157	UF
2005/02/02	21:50:16.8	37.80	43.89	08	3.8 ML	25 ± 5	3.60	3.16e+21	350	75	070	225	25	142	27	096	19	355	56	235	107	017	TF
2005/02/02[a]	23:26:53.4	37.75	43.62	08	4.6 mb	18 ± 4	4.11	1.84e+22	312	71	−137	205	50	−025	43	176	44	331	13	074	168	078	NS
2005/02/03	07:18:12.8	37.77	43.88	23	4.1 ML	25 ± 6	3.76	5.50e+21	025	68	118	150	35	040	19	095	26	194	57	334	088	178	TF
2005/10/31	17:42:48.7	34.31	45.45	10	4.1 ML	30 ± 8	4.27	3.20e+22	200	10	−070	360	81	−093	54	266	03	000	36	093	010	100	NF
2006/06/06[a]	17:03:05.0	35.69	46.04	30	5.0 mb	13 ± 3	4.21	2.60e+22	240	40	055	102	58	116	10	174	22	268	66	062	171	081	TF
2006/09/04	03:24:18.7	36.04	44.82	02	4.0 Mw	15 ± 3	3.82	6.76e+21	100	65	055	339	42	141	13	215	31	116	55	324	040	130	TF
2006/09/16[a]	08:54:21.7	35.29	45.40	80	4.5 mb	17 ± 5	3.92	9.55e+21	080	65	035	334	59	150	04	205	48	111	42	299	026	116	TS
2007/03/11	06:49:02.9	37.42	43.96	05	3.5 ML	16 ± 4	3.63	3.51e+21	169	63	127	290	45	040	10	233	33	330	55	128	049	139	TF
2007/05/07	13:52:17.3	37.69	43.88	05	3.9 ML	20 ± 5	3.74	5.13e+21	290	70	−025	029	67	−158	32	249	58	074	02	340	070	160	SS
2007/07/08	13:44:34.0	36.26	44.77	05	4.4 mb	18 ± 4	4.38	4.68e+22	080	80	005	349	85	170	04	035	79	143	11	304	035	125	SS
2007/09/18	20:53:32.1	35.61	44.63	40	4.3 ML	18 ± 4	4.32	3.80e+22	295	80	−035	032	56	−168	31	248	54	101	16	348	074	164	SS
2008/01/28	02:35:45.3	37.65	43.92	05	3.8 ML	32 ± 7	4.54	8.13e+22	024	85	−109	280	20	−015	47	274	19	026	37	131	061	151	UF
2008/02/18[a]	03:08:47.1	36.36	40.87	06	3.8 ML	15 ± 6	3.51	2.32e+21	320	85	−020	052	70	−175	18	274	69	127	10	007	096	006	SS
2008/04/15	06:56:34.4	37.33	44.55	02	3.6 ML	18 ± 4	3.48	2.09e+21	329	84	−114	225	25	−015	46	214	24	331	34	079	007	097	UF
2008/05/05	11:45:23.1	35.77	43.62	04	3.8 MD	11 ± 2	3.34	1.29e+21	045	65	000	135	90	−155	17	003	65	135	17	267	000	090	SS
2008/05/11[a]	23:20:07.7	37.36	43.20	40	4.1 ML	17 ± 5	3.89	8.61e+21	070	75	−025	167	66	−164	28	027	61	221	06	120	029	119	SS
2008/06/25[b]	03:05:37.4	37.62	43.79	05	4.2 MN	17 ± 4	4.30	3.55e+22	009	76	−164	275	75	−015	21	232	69	051	00	142	052	142	SS
2008/07/05[a]	19:00:18.7	36.22	42.25	03	3.6 MD	14 ± 4	3.22	8.51e+20	218	86	−145	125	55	−005	27	087	55	224	21	346	081	171	UF
2008/08/01	15:16:21.7	37.59	44.05	05	3.9 ML	22 ± 9	3.84	7.24e+21	035	81	150	130	60	010	14	086	59	201	27	348	083	173	SS
2008/11/30	16:57:29.7	37.54	44.68	02	3.7 ML	20 ± 6	3.93	9.89e+21	060	73	148	160	60	020	08	112	54	214	34	016	110	020	SS
2008/12/01	10:18:38.0	35.29	46.17	16	5.0 mb	14 ± 3	4.00	1.26e+22	320	05	115	115	85	088	40	207	02	115	49	023	036	126	UF
2008/12/14[a]	16:23:41.4	36.01	44.95	10	3.8 ML	17 ± 5	3.70	4.47e+21	163	77	−149	065	60	−015	31	028	57	183	11	291	024	114	SS
2009/03/01[a]	20:53:30.6	36.89	42.17	02	3.9 ML	14 ± 4	3.63	3.51e+21	268	80	129	010	40	015	25	329	38	081	41	215	139	049	UF
2009/03/10	13:13:01.8	37.18	43.66	02	4.2 ML	21 ± 7	4.52	7.59e+22	223	86	−140	130	50	−005	30	095	50	228	24	350	087	177	UF
2009/04/23[a]	00:26:22.5	37.00	42.62	10	3.8 ML	20 ± 6	3.62	3.39e+21	160	80	−025	255	65	−169	25	115	63	320	10	209	118	028	SS
2009/05/01	16:32:12.9	37.63	43.93	02	3.8 ML	22 ± 5	3.67	4.03e+21	200	65	050	083	46	144	11	318	36	220	52	062	142	052	UF
2009/05/08[b]	17:51:22.0	37.62	43.84	05	3.7 MN	20 ± 9	3.44	1.82e+21	218	77	−106	090	20	−040	55	109	15	222	31	321	064	154	NF
2009/07/18	20:32:27.3	35.76	43.34	10	5.1 Mw	09 ± 2	4.71	1.46e+23	245	75	010	152	80	165	04	199	72	301	18	108	018	108	SS
2009/09/20[a]	20:14:47.1	36.27	40.85	10	3.9 ML	14 ± 4	3.59	3.05e+21	054	76	−164	320	75	−015	21	277	69	096	00	187	097	007	SS
2010/01/07[a]	17:46:10.6	36.43	41.22	05	3.5 ML	24 ± 6	3.32	1.20e+21	330	65	055	209	42	141	13	085	31	346	55	194	090	000	TF
2010/05/07[a]	14:21:37.4	36.49	42.82	11	3.6 ML	23 ± 5	3.46	1.95e+21	234	72	−154	135	65	−020	31	096	58	266	05	003	094	004	SS
2010/08/08[a]	17:35:17.7	36.84	45.15	10	4.1 mb	20 ± 6	3.34	1.29e+21	275	70	−025	014	67	−158	32	234	58	059	02	325	055	145	SS
2010/11/22[a]	10:38:02.0	36.98	42.86	05	4.2 ML	20 ± 7	4.01	1.30e+22	067	81	160	160	70	010	07	115	68	223	21	022	114	024	SS

Table 1

continued

Date	O. time (UTC)	Lat. *N*	Log. *E*	RD (km)	M	CD (km)	M_W	Mo dyne-(cm)	Plane 1			Plane 2			Moment stress axes						S_H	S_h	Stress regime
									S	*D*	*R*	*S*	*D*	*R*	*P*		*N*		*T*				
															PL	AZ	PL	AZ	PL	AZ			
2011/01/02	13:14:20.2	36.75	43.23	20	4.2 mb	17 ± 4	3.75	5.31e+21	300	70	−030	041	62	−157	35	258	54	089	05	352	080	170	SS
2011/03/16	18:46:06.0	34.96	45.55	30	4.2 mb	18 ± 8	3.84	7.24e+21	115	65	040	005	54	149	06	238	44	142	45	335	060	150	TS
2011/04/06	19:17:19.0	34.36	45.71	15	4.6 mb	32 ± 9	4.20	2.51e+22	195	10	−065	350	81	−094	54	255	04	350	36	083	001	091	NF
2011/04/07	04:47:40.0	34.14	45.71	40	4.6 mb	34 ± 4	4.31	3.67e+22	185	75	−080	331	18	−123	59	109	10	002	29	267	168	078	NF
2011/04/07	05:16:13.1	34.44	45.49	05	4.1 ML	28 ± 9	3.83	7.00e+21	175	15	−090	355	75	−090	60	265	00	355	30	085	175	085	NF
2011/04/08	04:27:46.0	34.14	45.78	15	4.3 ML	30 ± 7	4.19	2.43e+22	180	15	−080	350	75	−093	60	256	03	350	30	082	175	085	NF
2011/05/27	12:31:08.0	36.72	45.00	02	4.1 ML	21 ± 6	3.64	3.63e+21	075	90	−025	345	65	180	17	207	65	075	17	303	030	120	SS
2011/05/29	11:02:06.0	37.35	42.55	05	4.5 mb	12 ± 3	4.39	4.84e+22	319	85	165	050	75	005	07	005	74	121	14	273	004	094	SS
2011/05/29[a]	14:30:11.0	37.32	42.55	02	3.7 ML	21 ± 5	3.24	9.12e+20	185	75	−045	290	47	−159	42	137	43	350	17	243	147	057	NS
2011/06/06	19:25:55.0	36.46	44.03	08	3.9 ML	20 ± 5	3.37	1.43e+21	195	15	−010	295	87	−105	46	190	15	295	41	038	154	064	UF
2011/10/27[a]	08:04:22.0	37.21	43.93	10	5.1 mb	19 ± 3	4.69	1.36e+23	215	90	070	125	20	180	42	324	20	215	42	106	171	081	UF
2011/10/28	18:42:07.0	37.40	44.31	05	3.6 ML	18 ± 5	3.35	1.33e+21	234	63	127	355	45	040	10	298	33	035	55	193	114	024	TF
2011/12/06[a]	15:46:28.0	37.30	43.94	02	4.5 ML	15 ± 4	4.15	2.11e+22	139	81	−155	045	65	−010	24	005	63	158	11	270	002	092	SS
2012/02/03	22:47:28.0	34.77	45.62	10	3.6 ML	09 ± 2	3.32	1.20e+21	300	35	−055	079	62	−112	66	310	19	090	14	185	100	010	NF
2012/03/05[a]	06:50:34.0	35.04	44.09	02	4.7 mb	25 ± 6	4.83	2.21e+23	145	70	080	352	22	116	24	243	09	148	64	039	069	159	TF
2012/04/24[a]	23:28:53.0	37.42	44.75	02	3.8 ML	15 ± 4	3.77	5.69e+21	306	76	−154	210	65	−015	28	170	61	332	08	076	168	078	SS
2012/05/05[a]	01:57:13.0	35.10	44.16	15	4.4 mb	22 ± 5	4.76	1.74e+23	186	87	110	285	20	010	38	258	20	004	45	115	056	146	UF
2012/05/21	11:57:56.0	36.41	43.18	11	3.8 ML	21 ± 6	3.50	2.24e+21	050	05	−010	150	89	-095	46	055	05	150	44	245	008	098	UF
2012/06/14	05:52:54.0	37.21	42.47	10	5.3 mb	19 ± 5	5.30	1.12e+24	055	85	−055	152	35	−171	40	357	35	232	31	117	014	104	UF
2012/06/15[a]	23:48:15.0	37.20	42.44	02	4.2 ML	14 ± 4	4.22	2.69e+22	210	80	−015	303	75	−170	18	166	72	357	03	257	166	076	SS
2012/06/16	02:10:07.0	37.20	42.43	02	3.9 ML	15 ± 6	3.70	4.47e+21	200	90	−045	290	45	−180	30	145	45	020	30	255	155	065	UF
2012/06/16[a]	03:12:55.0	37.19	42.45	02	3.7 ML	14 ± 4	3.50	2.24e+21	035	80	025	300	65	169	10	166	63	055	25	260	168	078	SS
2012/06/16	03:22:58.0	37.18	42.47	02	3.9 ML	15 ± 3	3.68	4.17e+21	154	85	165	245	75	005	07	200	74	316	14	108	019	109	SS
2012/06/22	23:43:20.0	37.18	42.57	02	3.5 ML	23 ± 6	3.35	1.33e+21	355	85	010	264	80	175	03	129	79	021	11	220	129	039	SS
2012/08/05	20:37:23.0	37.44	42.93	10	5.1 Mw	20 ± 8	5.05	4.27e+23	228	61	−132	110	50	-040	53	085	36	253	06	347	079	169	NF
2012/09/12[a]	23:29:38.0	37.21	43.57	02	4.2 ML	22 ± 7	4.14	2.04e+22	055	25	−020	163	82	−114	48	048	23	167	33	273	019	109	UF
2012/09/13[a]	02:42:21.0	36.99	43.72	02	4.2 ML	13 ± 5	4.39	4.84e+22	060	85	−020	152	70	−175	18	014	69	227	10	108	016	106	SS
2013/03/11	14:57:09.0	36.64	43.55	10	5.0 mb	16 ± 4	5.00	3.98e+23	310	70	−015	045	76	−159	24	269	65	078	04	177	088	178	SS
2013/03/13	06:23:03.0	36.66	43.38	10	4.3 mb	19 ± 6	4.47	6.38e+22	295	90	−070	025	20	−180	42	224	20	115	42	006	071	161	UF

The horizontal stress axes and stress regimes were calculated from moment stress axes according to Zoback (1992) and Lund and Townend (2007)

O time (*UTC*) original time in UTC, *Lat* latitude in degree, *Log* longitude in degree, *RD* reported depth in km, *M* reported magnitude, *CD* calculated depth in km, *Mw* moment magnitude, *Mo* seismic moment measured in dyne-cm, *S* strike, *D* dip, *R* rake angle, *P*, *N*, and *T* compressional, normal, and tensional moment stress axes, respectively, *PL* plunge angle, *AZ* azimuth, S_H maximum horizontal stress axis, S_h minimum horizontal stress axis, *NF* normal faulting, *NS* normal faulting with strike-slip component, *SS* strike-slip faulting, *TS* thrust faulting with strike-slip component, *TF* thrust faulting, *UF* unknown or oblique faulting

[a] Focal mechanism solutions are from Abdulnaby *et al.* (2013)

[b] Source parameters are from Iranian Seismic Network (ISN) catalog

(N) axis represents the neutral axis that has no shortening or extension, and it is located at the intersection of the fault and auxiliary planes. Moment stress axes are perpendicular to each other. The angle between the P and T axis and the fault plane or the auxiliary plane is assumed to be 45° according to Anderson (1951).

5.3. Horizontal Stress Axes

The horizontal stress axes are the maximum horizontal stress axis (S_H) and the minimum horizontal stress axis (S_h), which are perpendicular to each other. The vertical stress axis (S_V) is perpendicular to the horizontal stress axes (S_H and S_h). The horizontal stress is the most dominant stress due to the horizontal plate driving mechanism. Therefore, the best way to display the tectonic stress is to map the azimuth of the horizontal stress. Two methods to calculate the horizontal stress axes are explained in the following discussion.

5.3.1 Horizontal Stress from the Moment Stress Axes

Zoback (1992) provided a simple method to calculate S_H from the moment stress axes (P, N, and T). As shown in Table 3 in Zoback (1992); in the case of a pure normal faulting regime (NF), the S_H orientation is taken as the azimuth of the N axis. In the case of a pure thrust faulting regime (TF), the S_H orientation is taken as the azimuth of the P axis. In the case of a normal faulting with strike-slip component (NS), when the N axis generally plunges more steeply than the T axis, the S_H orientation is taken as the azimuth of T axis plus 90° (Zoback 1992).

5.3.2 Horizontal Stress from the Four Stress Tensors

Lund and Townend (2007) developed a mathematical method to compute the true direction of the horizontal stress axes from the four stress tensor components (σ_1, σ_2, σ_3, and R) that are obtained from the inversion of focal mechanism data. This method is applied in the TENSOR program; and it is used in this study to calculate the S_H and S_h (for details see equation 11 and Table 2 in Lund and Townend 2007).

The two methods were applied to calculate the orientations of S_H and S_h for each focal mechanisms; and the results were identical in most cases (Table 1). Figure 3 shows the orientations of the S_H and S_h stress axes. The horizontal stress axes are presented in term of S_H for thrust, strike-slip, and oblique faulting regimes and S_h for normal faulting regimes.

5.4. Tectonic Stress Regimes

The tectonic stress regime explains the relation between the style of faulting and the orientation of the stress axes. Anderson (1951) reported the most famous classification of tectonic stress regimes in the lithosphere. Zoback (1992) developed Anderson's classification to have six categories of tectonic stress regime. This classification is based on the plunge angle (Θ) of the moment stress axes (P, N, and T), principal stress axes (σ_1, σ_2, and σ_3), or horizontal stress axes (S_H, S_V, and S_h). The six categories are: normal faulting (NF), normal faulting with strike-slip component (NS), strike-slip faulting (SS), thrust faulting with strike-slip component (TS), and thrust faulting (TF). The data which fall outside these categories are assigned to an unknown or oblique stress regime or faulting (UF) and indicate that the maximum horizontal stress azimuth is not defined.

The tectonic stress regime of each focal mechanism was estimated based on Zoback (1992, Table 3). Figure 4 illustrates the distribution of stress regimes of the study area based on Table 1. The results show that all six categories of the stress regimes exist. However, the most common tectonic regimes in the study area are the SS (43.94 %), UF (27.27 %), and TF (13.64 %), as compared to the less frequent stress regimes of NF (9.09 %), NS (3.03 %) and TS (3.03 %) in the area. In most cases, the strike-slip movement on the fault surfaces consists of left-lateral (sinistral) movement.

5.5. Formal Stress Inversion

The moment stress axes from earthquake focal mechanisms do not coincide with the principal stress axes, because earthquakes typically occur on pre-existing faults in a heterogeneous anisotropic medium such as the crust (see, e.g., Scholtz 2002; Stein and Wysession 2003). However, the maximum principal stress axis (σ_1) still lies within the dilatational

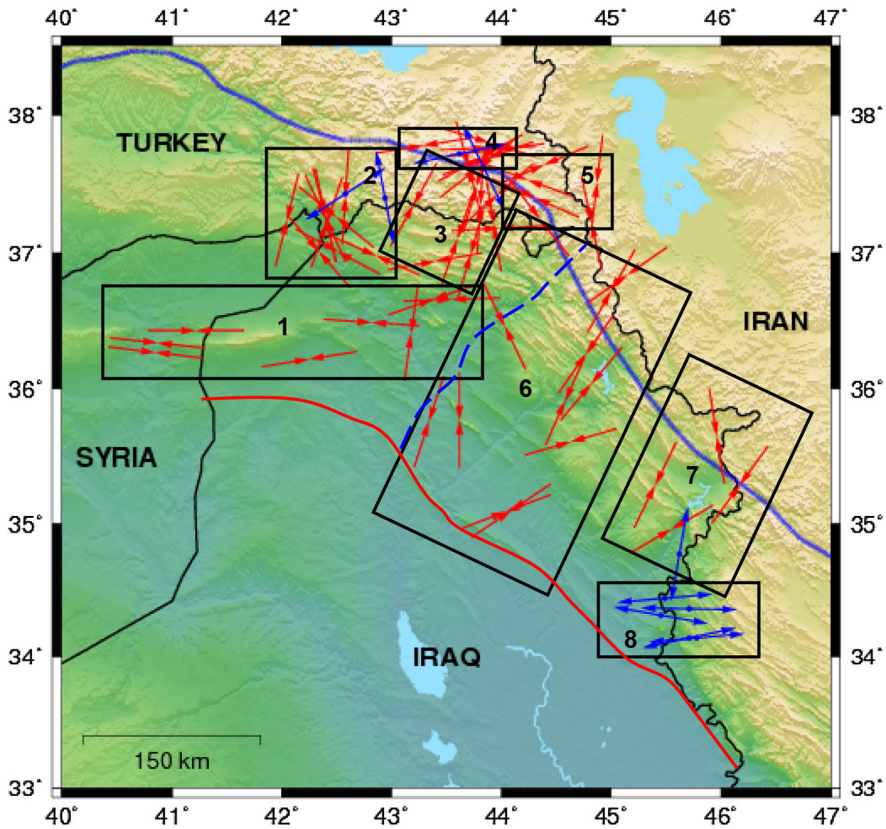

Figure 3
Horizontal stress axes in northern Iraq and surrounding regions from the focal mechanism solution based on Table 1. The maximum horizontal stress axes (S_H) are presented in *red arrows* for thrust, strike-slip, and oblique faulting regimes, while the minimum horizontal stress axes (S_h) are presented in *blue arrows* for normal faulting regimes. These axes were grouped into eight sub-areas for formal stress inversion

Table 2

Results of formal stress inversion of the rotational optimization method for the eight sub-areas

Subarea definition			Reduced stress tensor parameters							Horizontal stress axes		Stress regime	Quality
No	Location	No. of data	σ_1		σ_2		σ_3		R	S_H	S_h		
			PL	AZ	PL	AZ	PL	AZ					
1	Mosul	8	08	267	79	127	07	358	0.77	088	178	SS	B
2	Duhok-Sirnak	12	11	144	69	023	17	237	0.53	146	056	SS	B
3	Duhok-Hakkari	8	27	024	60	173	13	287	0.39	020	110	SS	B
4	Hakkari	10	20	084	55	204	28	343	0.27	079	169	UF	C
5	Orumiyeh	6	00	126	84	035	06	216	0.01	126	036	SS	C
6	Erbil-Kirkuk	11	25	234	64	038	06	141	0.13	052	142	SS	B
7	Sulaymaniyah	5	17	229	45	122	40	334	0.36	055	145	UF	C
8	Diyala	5	56	261	03	355	33	086	0.40	000	090	NF	B

quadrant of the focal mechanism (McKenzie 1969), which means the focal mechanism solution does restrict the maximum compression direction to a range of possible angles. To derive the orientation of the principal stress axes from moment stress axes, a formal stress inversion method needs to be

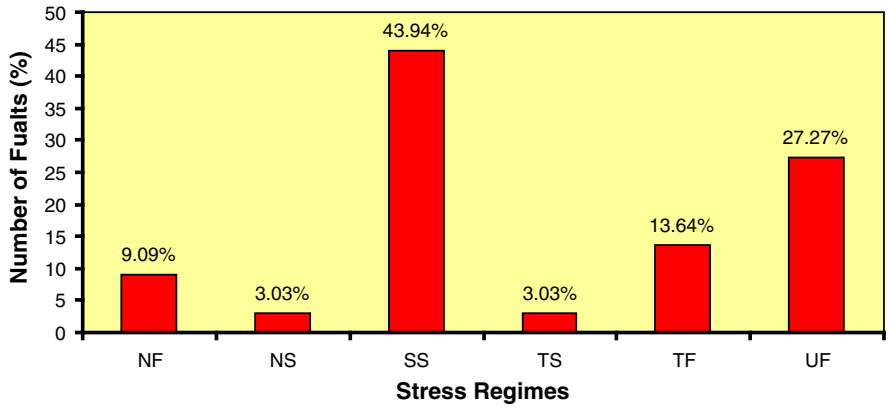

Figure 4
Distribution of stress regimes in northern Iraq and surrounding regions from focal mechanism data (see Table 1)

performed. A major difference between stress inversion techniques is the handling of the focal mechanism ambiguity concerning determination of the focal and auxiliary planes from the two nodal planes in order to define the actual fault plane. Some algorithms need the fault plane to be determined a priori. The advantage of the TENSOR method is that the determination of the fault plane is made during the process and not a priori (Delvaux and Barth 2010).

The study area was divided into eight rectangular sub-areas (boxes) to study regional changes in stress orientation since the stress regime and stress orientation over the entire study area are not consistent, thus, it cannot invert altogether (Barth 2007). We have tested the sensitivity of the box boundaries. We have three major different tectonic regions in the area that we used as a base for choosing the boxes boundaries. These are: Kirkuk block, Mosul block, and Eurasian plate. In addition to that the eight subareas were demarcated according to the consistency of the moment stress axes directions and the fracture types in each one of them. We have chosen different distribution of boxes within each one of these tectonic regions, and the results were the same.

These sub-areas were named according to the city names and geographical locations included in each one of them; they are from sub-area 1 to sub-area 8: Mosul (Ninevah), Dohuk-Sirnak, Dohuk-Hakkari, Hakkari, Orumiyeh, Erbil-Kirkuk, Sulaymaniyah, and Diyala (Fig. 3).

After the subdivision of the study area, the focal mechanism solutions within each sub-area were inverted by the New Right Dihedron method and the Rotational Optimization method. In summary, the steps that we followed to derive the principal stress axes and stress ratio from moment stress axes are as follows:

1. Use the stress tensor estimated by the New Right Dihedron method as a starting point to restrict the search area during the inversion, so that the whole grid does not have to be searched.
2. Invert both nodal plans for each focal mechanism to stress tensor. Then the plane that has the smaller value of a misfit function called F5, which is calculated from the iterative grid search, will be selected as the actual fault (or focal) plane.
3. Invert only the focal planes that are best fitted by a uniform stress field to define the three principal stress axes and calculate the stress ratio.

The graphical output of the stress inversion by TENSOR program depicts the projection of the principal stress axes in a lower hemisphere equal-area projection and allows evaluating the overall quality of the result (Delvaux and Barth 2010). The results of these inversions are shown in Fig. 5 and Table 2. The horizontal stress axes (S_H and S_h) for the eight zones were plotted on a map as shown in Fig. 6. The locations of the horizontal stress axes on the map represent the geometric center of each rectangular sub-area.

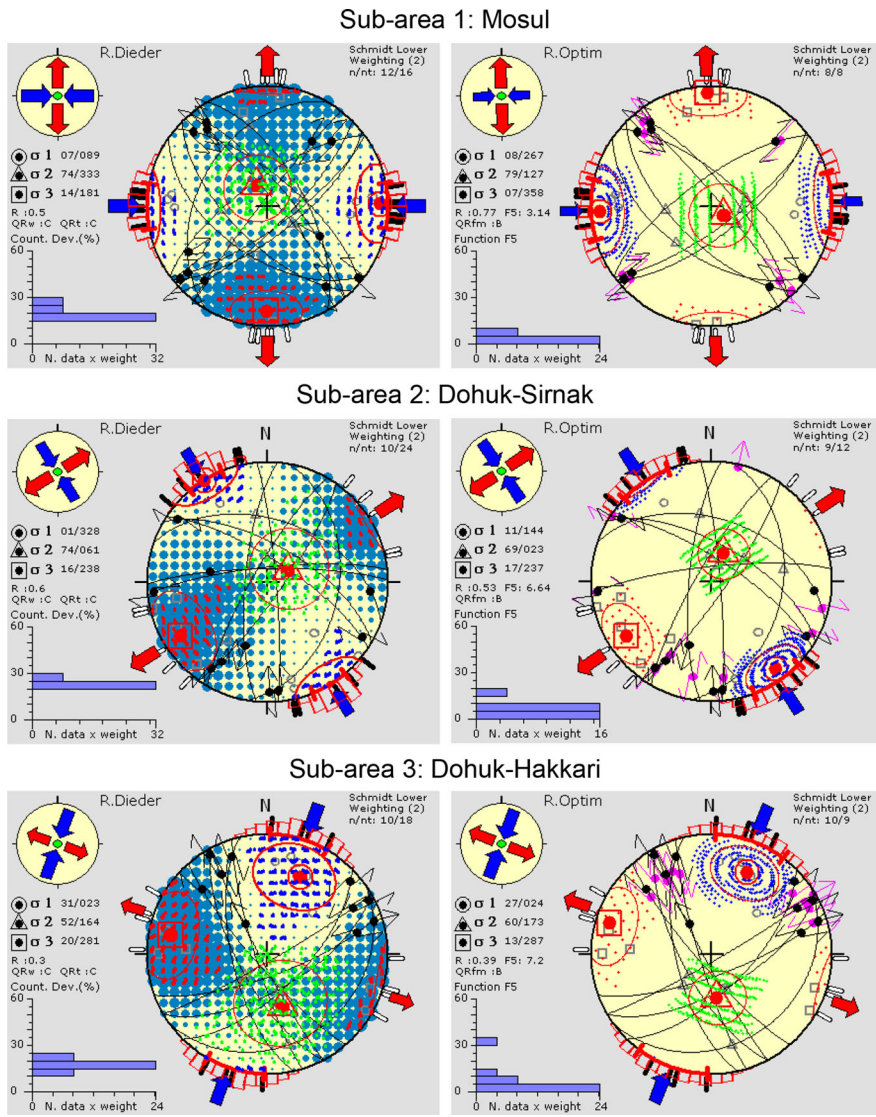

Figure 5
Formal stress inversion of the eight sub-areas by the New Right Dihedron method (*left panels*) and the Rotational Optimization method (*right panels*)

Figure 5 represents the lower-hemisphere equal-area stereographic projections of the focal mechanism solutions of the eight sub-areas. For each sub-area, the left panel is the result of applying the Right Dihedron Method, while the right panel is the result of applying the Rotational Optimization method. The selected focal planes are shown as great circles and associated slip lines as black dots with outward arrows. Stress inversion results are represented by the orientation of the three principal stress axes, each of which is represented by a red dot surrounded by a circle for σ_1, a triangle for σ_2, and a square for σ_3. The related horizontal stress axes are represented by a large blue arrow outside the stereogram for S_H and a red arrow for S_h. The orientations of the related moment stress axes are depicted by a small gray circle for the *P*-axis, a triangle for the *N*-axis, and a square for the *T*-axis. The directions of the horizontal stress axes are represented by the black bars on the periphery of the stereogram for the S_H and white bars

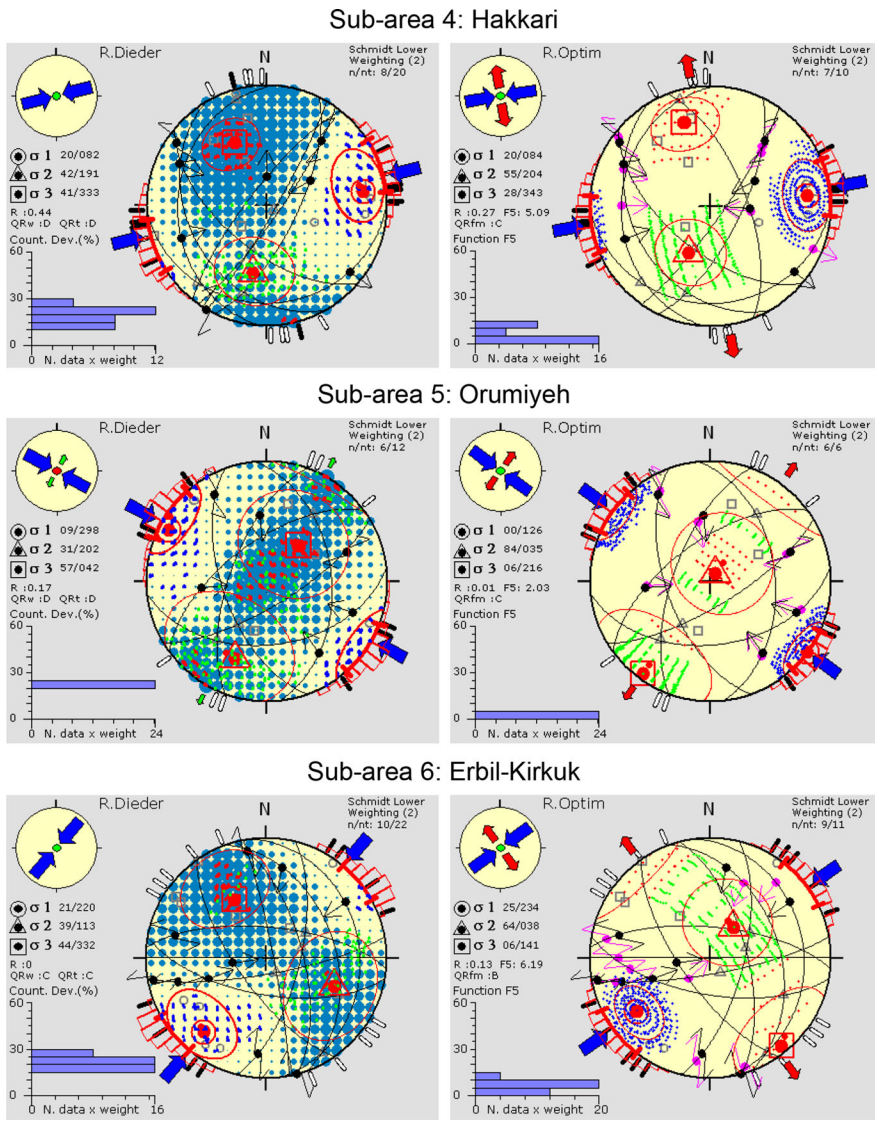

Figure 5
continued

for S_h for individual focal mechanisms. The small circle on the upper left corner of each panel shows the direction and type of the horizontal stress axes. The histograms to the lower left corner of the stereograms depict the distribution of the misfit angle F5 in the TENSOR program weighted arithmetically according to the magnitude for each case.

A quality ranking scheme of stress orientations determined from focal mechanisms was developed by Zoback and Zoback (1989, 1991) and Zoback (1992) and updated by Sperner *et al.* (2003). Five qualities are used in ranking the data, which are between *A* and *E*, with *A* being the highest quality and *E* the lowest. The ranking criteria include accuracy of the measurements, the number of determinations, and the magnitude cutoff. Higher-quality rankings are assigned to the larger earthquakes (Zoback 1992). The focal mechanism data from an individual earthquake has *C*, *D*, or *E* quality data since the *P*, *N*, and *T* axes might be different from the actual stress

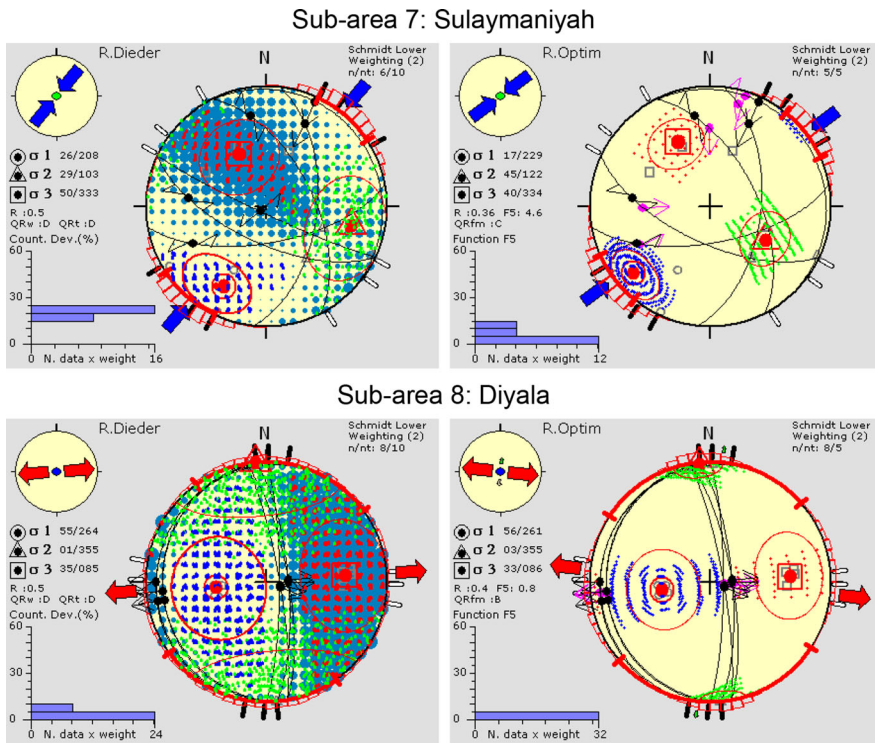

Figure 5
continued

orientations. An *A* or *B* quality cannot be given to a single focal mechanism even if the solution is well constrained and the event has high magnitude. The misfit angle is $\leq 12°$ for *A* quality, $\leq 20°$ for *B* quality, and $\leq 25°$ for *C* quality. The quality of our stress inversions for the eight sub-areas was determined to be of *B* and *C* quality as shown in Table 2.

6. Discussion

6.1. Sub-Area Boundaries

Six of the eight demarcated sub-areas are located on the tectonic blocks of Kirkuk and Mosul. Each of the two tectonic blocks has three sub-areas within it (sub-areas 1, 2 and 3 on the Mosul Block and 6, 7 and 8 on the Kirkuk Block). The two other sub-areas (4 and 5) are located in the Eurasian (Iranian) plate near the Bitlis–Zagros suture line. The selection of the sub-areas boundaries was made to define contiguous areas that are characterized by the greatest density of similar focal mechanisms. These sub-areas were approximated to be rectangular for simplicity on the map.

6.2. Derived Horizontal Stress Axes Versus the World Stress Map

In the World Stress Map project, the horizontal stress axes are usually used to express the tectonic regimes. The horizontal stress axes are presented in term of S_H for thrust, strike-slip, and oblique faulting regimes and S_h for normal faulting regimes. Our stress inversion results reveal a general trend of NE–SW compression for most of the Kirkuk Block (sub-areas 6 and 7) and E–W, NW–SE, and N–S (sub-areas 1, 2, and 3 respectively) for most of the Mosul Block (Fig. 6). According to the World Stress Map (HEIDBACH *et al.* 2008), two stress regimes are represented in the study area; these are the strike-slip faulting regime that is located in the collision zone between Arabian and Turkish plates, and the thrust faulting

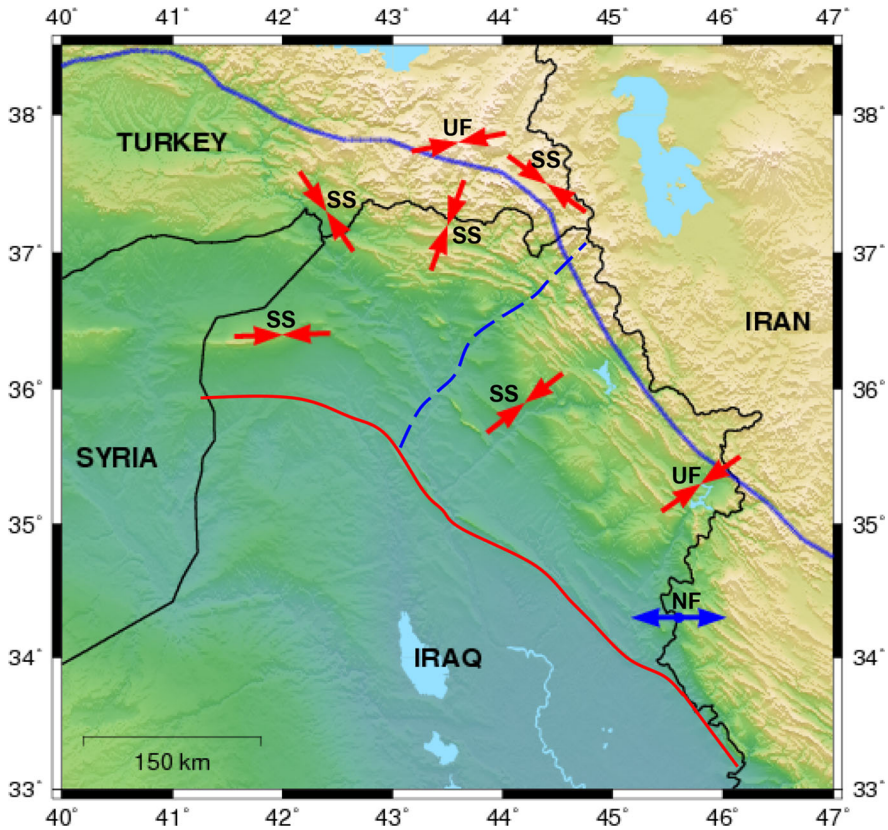

Figure 6
The horizontal stress axes in northern Iraq and surrounding regions from the formal stress inversion methods of the eight sub-areas based on Table 2. The maximum horizontal stress axes (S_H) are presented in red arrows for the strike-slip and oblique faulting regimes, while the minimum horizontal stress axes (S_h) are presented by *blue arrows* for normal faulting regime

regime that is located in the collision zone between Arabian and Iranian plates. Our results tend to support the World Stress Map. However, in our study we found the strike-slip and oblique faulting regimes besides the thrust faulting regime at the collision zone between the Arabian and Iranian plates as well. These types of faulting are the results of the anticlockwise rotation of Arabia as will be explained more lately.

6.3. *Comparison with Paleostress Axes*

Only a few studies have been carried out to describe the paleostress regime in northern Iraq and surrounding regions. NUMAN (1984) reported that there were two regional components of compression at the Arabian-Eurasian continental collision zone. One is parallel to the suture of the collision zone and is responsible for the presently dominant wrench tectonism in the area, and the second is perpendicular to the suture and leads to shortening across the orogenic belt, which is responsible for reverse faulting and folding. This geodynamic scenario is ongoing to the present day and is, thus, responsible for neotectonic and seismic activities in the studied region. Subsequent studies on brittle failure structures together with the analysis presented here from focal mechanism solutions have added more detail to the tectonic history of the studied area.

AL-JUMAILY (2004) and AL-JUMAILY and NUMAN (2009) studied the paleostress regime of the Foreland Fold Belt of northern Iraq by using the analysis of brittle failure structures, which include joints, faults, veins, and stylolites. This study found

that twelve states of paleostress have affected the area of northern Iraq from the End-Cretaceous to the End-Tertiary times. The paleostress regime has two directions of tectonic compression in northern Iraq; these are perpendicular (transverse) and parallel (longitudinal) to the fold axes of the Bitlis and Zagros trends. This study has shown a continuation of some of the established paleostress regimes to the present day. Furthermore, this study has shown that the strike-slip displacements predominate over reverse and normal displacements, suggesting that wrench tectonism was predominant in northern Iraq. Nevertheless, field evidence from all the major anticlinal structures in the study area indicate that in the early stages of folding wrench tectonism was not predominant in this area. This is evidenced by the presence of surface and subsurface major longitudinal reverse or normal faults—not strike-slip displacements—in the steeper limbs of these asymmetrical structures.

Sub-area 1 exemplifies the directional departure between the paleostress and present day stress since this study has shown that the present principal stress axis in this sub-area is oriented E–W; it is parallel to the axis of the gigantic Sinjar Anticline which is over 80 km long (not perpendicular or oblique to the anticlinal axis as one would expect and is the case in the other sub-areas in this study). However, a good degree of directional compatibility is seen between the direction of paleostresses and the direction of the present day principal stress axes which are still perpendicular to the fold axes in sub-areas 6, and 7 of the Kirkuk Block. This local variation of relationship between the directions of paleostresses obtained from previous studies and present day principal stress axes obtained from this study is believed to be related to the anticlockwise rotation of Arabia. Thus the variation can be interpreted in terms of the orientations of the Zagros and Bitlis collision zones, which are trending NW–SE and E–W consecutively, and the anticlockwise rotation of Arabia which would be enhanced in this dynamics and the geometrical setting of the NE–SW oriented compressional stresses in the Foreland Folds Belt in sub-areas 6 and 7, while it would introduce an E-W oriented compression in sub-area 1.

6.4. Tectonic Stress Regimes and Styles of Faulting

Strike-slip faulting is the most common style of faulting in the study area due to the anticlockwise rotation of the Arabian plate. The oblique faulting style is the result of interaction between the vertical basement block movements brought about by the reactivation of the listric faults mentioned above, and the horizontal stress axes, which were found in this study. The peculiarity that has been revealed in this study, of having normal faulting (i.e., tensional stresses near the Iraq-Iran border) in sub-area 8 which is surrounded by a compressional stress regime can be explained in terms of local tensional stresses that develop in areas of strike-slip displacements, as suggested by Numan (2000). This is similar to the mechanism of pull-apart basin formation described by Smit *et al*. (2008) in the Dead Sea. However, this sub-area is not well-constrained due to the low number of data used; nevertheless, these inversions can give an important indication for the understanding of the stress pattern as a whole. Similar studies had also performed stress inversions for boxes with five and six FMSs (e.g., Delvaux and Barth 2010). Therefore, we recommend that more focal mechanism solutions to be calculated and used for the stress inversion. The results of inversion do not show the thrust faulting regime being dominant in any of the eight sub-areas despite the fact that it represents 13.64 % of the whole faulting styles. That is due to the dispersion of this type of faulting within the eight sub-areas rendering it subordinate in occurrence.

6.5. Tectonic Stress Fields

A tectonic stress field describes the way that the tectonic stress regime varies through space in a body (Zang and Stephansson 2010). In general, the distribution of tectonic stress is directly associated with plate movement and also with variations from place to place. According to Zoback (1992), Heidbach *et al*. (2007, 2010), the tectonic stress field can be classified as a function of the spatial scale of investigation into three orders; these are first order, second order, and third order stress fields. Our study area of northern Iraq and surrounding regions has the three order stress fields. The first stress order is

related to the convergent plate movement and mostly controlled by the geometry of plate boundaries and the forces acting on plate boundaries. The relation between the plate motions and the stress field in a region explains why the orientation of horizontal stress, at the plate scale, is predominately subparallel to the absolute or relative plate motions. The second order stress field is controlled by regional block interaction. This is manifested in our study area by two major basement blocks which are the Mosul and Kirkuk blocks. The third order stress fields are inferred from the existence of a large number of smaller basement blocks which control the formation of the major anticlinal structures in the study area. Sub-area 8 is an example of a small block responding to the locally developed stress field.

7. Conclusions

We show that using focal mechanism data from 65 earthquakes in northern Iraq and surrounding regions can resolve the stress pattern by formal stress inversion. The moment tensor inversion method was used to estimate the focal mechanisms. For stress inversion, two methods were used; these are the Improved Right Dihedron Method and Rotational Optimization.

The pattern of present-day tectonic stress fields in northern Iraq and surrounding regions is controlled by the dynamics of the collision between the Arabian and Eurasian plates. Our analyses show the existence of six categories of stress regimes in the study area. These are normal faulting (NF), normal faulting with strike-slip component (NS), strike-slip faulting (SS), thrust faulting with strike-slip component (TS), thrust faulting (TF), and unknown or oblique faulting (UF). However, the most common tectonic regimes in the study area are the SS (43.94 %), UF (27.27 %), and TF (13.64 %); the less common tectonic regimes are the NF (9.09 %), NS (3.03 %), and TS (3.03 %). In most cases, the nature of strike-slip displacement on fault surfaces is left-lateral (sinistral). The NF regime, which is located in sub-area 8 near the city of Diyala at the Iraq-Iran border, represents a local tensional stress regime. This is thought to be a local pull-apart area of wrench tectonics within an essentially compressional environment.

The directions of the obtained compressional principal stress axes in this study show that the compressional stress regime at the Bitlis–Zagros suture zone has two directions. One is perpendicular to the suture near the Iraq–Iran border, and the second is parallel in places as well as perpendicular in others to the suture near the Iraq–Turkey border. In addition, the compressional principal stress axes in the sub-area 8 in the Sinjar area near the Iraq–Syria border have an E–W direction. These results are compatible with the tectonic setting of the Arabian–Eurasian continental collision zone and the anticlockwise rotation of the Arabian plate which appears responsible for strike-slip displacements on fault surfaces.

Acknowledgments

We thank Dr. Robert Herrmann of SLU for the CPS software package, Delvaux and Sperner for the TENSOR program, and Wessel and Smith for the GMT software. Also, we thank Albert Everett of UALR Graduate Institute of Technology for his continuous involvement and help with the software installation and execution. Thanks go to IRIS, KOERI, ISN, and EMSC for the seismic data and catalog.

References

Abdulnaby, W., Mahdi, H., and Al-Shukri, H. (2012), Crustal structure from joint inversion of receiver function and surface wave dispersion beneath Duhok, NW Iraq, International Geophysical Conference and Oil & Gas Exhibition, Istanbul, Turkey, September 2012.

Abdulnaby, W., Mahdi, H., Numan, N. M. S., and Al-Shukri, H. (2013), *Seismotectonics of the Bitlis–Zagros Fold and Thrust Belt in northern Iraq and surrounding regions from moment tensor analysis*. Pure and Applied Geophysics, *170*, doi:10.1007/s00024-013-0688-4

Al-Jumaily, I. S. (2004), Tectonic investigation of the brittle failure structures in the Foreland Folds Belt – northern Iraq, Unpublished dissertation, College of Science University of Mosul/Iraq, 328P.

Al-Jumaily, I. S., and Numan, N. M. S. (2009), *Tectonic of Quaternary travertine accumulation at Al-Fatha area in middle Iraq*. Bulletin of the Mineral Research and Exploration, *138*, 1–7.

Alsinawi, S. A., and Al-Heety, E. A. (1994), *Crustal thickness determination in Iraq from long-period P-wave spectra*, Iraqi Geol. J., *25*, 28–49.

Anderson, E. M. (1951), The dynamics of faulting and dyke formation with applications to Britain. Oliver and Boyd, Edinburgh, 206 pp.

Angelier, J., and Mechler, P. (1977), *Su rune méthode graphique de recherché des contraintes principales également utilisable en tectonique et en seismologie : la méthode des diédres droits*. Bulletin de la Société Géologique de France, *7*(19), 1309–1318.

Barth, A. (2007), Frequency sensitive moment tensor inversion for light to moderate magnitude earthquakes in eastern Africa and derivation of the regional stress field. PhD thesis, University of Karlsruhe.

Delvaux, D. (1993), The TENSOR program for paleostress reconstruction: examples from the east African and the Baikal rift zones. In: Terra Abstracts. Abstract supplement No. 1 to Terra Nova, 5, 216.

Delvaux, D., and Barth, B. (2010), *African stress pattern from formal inversion of focal mechanism data*. Tectonophysics, *482*, 105–128.

Delvaux, D., and Sperner, B. (2003), Stress tensor inversion from fault kinematic indicators and focal mechanism data: the TENSOR program. In: Nieuwland, D. (Ed.), New Insights into Structural Interpretation and Modelling: Geol. Soc. Lond. Spec. Publ., vol. 212, pp. 75–100.

Heidbach, O., Reinecker, J., Tingay, M., Müller, B., Sperner, B., Fuchs, K. and Wenzel, F. (2007), *Plate boundary forces are not enough: Second and third order stress patterns highlighted in the World Stress Map database*, Tectonics, *26*: doi:10.1029/2007TC002133

Heidbach, O., Tingay, M., Barth, A., Reinecker, J., Kurfeß, D., and Müller, B. (2008), The World Stress Map database release 2008, doi:10.1594/GFZ.WSM.Rel2008

Heidbach, O., Tingay, M., Barth, A., Reinecker, J., Kurfeß, D. & Müller, B. (2010), *Global crustal stress pattern based on the World Stress Map database release 2008*, Tectonophysics, *462*, doi:10.1016/j.tecto.2009.1007.1023

Herrmanm, R.B. and Ammon, C.J. (1997), *Faulting parameters of earthquakes in the New-Madrid, Missouri, Region*, Engineering geology, *46*, 299–311.

Herrmann, R. B., and Ammon, C. J. (2002), Computer programs in seismology, version 3.30. Saint Louis University, Missouri.

Herrmann, R. B., and Ammon, C. J. (2004), Source inversion, In: Computer programs in seismology, version 3.30, Saint Louis University, Missouri.

Lund, B., Townend, J. (2007), *Calculating horizontal stress orientations with full or partial knowledge of the tectonic stress tensor*, Geophys. J. Int. *270*, 1328–1335.

McKenzie, D. P. (1969), *The relation between fault plane solutions for earthquakes and the directions of the principal stresses*, Bull. Seismol. Soc. Am., *59*, 591–601.

Mooney, W. D., Laske, G., and Masters, G. (1998), *CRUST 5.1: a global crustal model at 5° × 5°*, J. Geophys. Res., *103*, 727–747.

Numan, N. M. S. (1984), *Basement controls of stratigraphic sequences and structural patterns in Iraq*, Geol. Soc. Iraq. Jour., *16*, 8–28.

Numan, N. M. S. (1997), *A plate tectonic scenario for the Phanerozoic succession in Iraq*. Iraqi Geological Journal, Vol. *30*, No. 2, 85–119.

Numan, N. M. S. (2000), *Major Cretaceous tectonic events in Iraq*, Raf. Journal Science, *11,* 3, 32–52.

Reilinger, R., et al. (2006), *GPS constraints on continental deformation in the Africa-Arabia-Eurasia continental collision zone and implications for the dynamics of plate interactions*, J. Geophys. Res., *111*, B05411, doi:10.1029/2005JB004051

Scholtz, C. H. (2002), The mechanics of earthquakes and faulting. Cambridge University Press, 2nd edition, 471P.

Smit, J., Brun, J. P., Cloetingh, S., and Ben-Avraham, Z. (2008). *Pull-apart basin formation and development in narrow transform zones with application to the Dead Sea Basin*, Tectonics, *27*, 6, doi:10.1029/2007TC002119

Sperner, B., Müller, B, Heidbach, O., Delvaux, D., Reinecker, J., and Fuchs, K. (2003), Tectonic stress in the Earth's crust: advances in the World Stress Map project. In: Nieuwland, D. A. (ed.) New Insights into Structural Interpretation and Modelling. Geological Society, London, Special Publications, 212, 101–116.

Stein, S., and Wysession, M. (2003), An introduction to seismology, earthquakes, and earth structure, Blackwell Publishing, 3rd edition, 498P.

Zang, A., and Stephansson, O. (2010), Stress field of the Earth's crust, Springer, Netherlands, 322P.

Zoback, M. D., and Zoback, M. L. (1991), Tectonic stress field of North America and relative plate motions, in The Geology of North America, Decade Map vol. 1, Neotectonics of North America, edited by B. Slemmons et al., pp. 339–366, Boulder, Colo.

Zoback, M. L. (1992), *First- and second-order patterns of stress in the lithosphere: The World Stress Map Project*. Journal of Geophysical Research, *97*, 11703–11728.

Zoback, M. L., and Zoback, M. D. (1989), *Tectonic stress field of the conterminous United State*, Mem. Geol. Soc. Am., *172*, 523–539.

(Received August 21, 2013, revised March 3, 2014, accepted March 4, 2014)